Fabrication of a Meniscus Microlens Array Made of Anodic Alumina by Laser Irradiation and Electrochemical Techniques

Tatsuya Kikuchi*, Yuhta Wachi, Taka-aki Takahashi, Masatoshi Sakairi, and Ryosuke O. Suzuki
Faculty of Engineering, Hokkaido University
N13-W8, Kita-ku, Sapporo, Hokkaido, 060-8628, Japan

*Corresponding author: Tatsuya Kikuchi
TEL: +81-11-706-6340
FAX: +81-11-706-6342
E-mail: kiku@eng.hokudai.ac.jp

Abstract

An anodic alumina microlens array was fabricated by laser irradiation and electrochemical techniques. An aluminum specimen covered with a porous oxide film was irradiated with a pulsed Nd-YAG laser, and then electropolished to dissolve the aluminum substrate. A well-defined semi-elliptical micropore was formed on the aluminum by electropolishing. The immersion of the electropolished specimen in a CrO_3/H_3PO_4 solution resulted in the dissolution of the remaining anodic oxide film. Subsequent re-anodizing enabled the formation of a characteristic meniscus-shaped oxide film on the micropore. A microlens array made of the thin anodic alumina film, which showed flexibility and heat resistance, was successfully fabricated by the lift-off of the anodic oxide.

Key words: Aluminum; Anodizing; Laser Irradiation; Electropolishing; Microlens Array

1. Introduction

Micrometer-scale lens arrays have been widely investigated and fabricated for their incorporation into micro-optical devices such as liquid-crystal display (LCD) projectors, charge coupled device (CCD) image sensors, three-dimensional (3D) televisions, etc [1-5]. The fabrication techniques used to produce microlens arrays have already been reported by many researchers; typical techniques include the thermal reflow of photoresist materials [2, 6, 7], the gray-scale mask method [8-10], and the ion diffusion method [11]. These fabrication processes are typically based on photolithography with a resist coating, followed by soft baking, exposure, development, and post baking. However, because photolithography involves many steps with toxic reagents and is seldom applied to materials with 3D structures, such as stepped and curved surfaces, a technique for fabricating microlens arrays without using photolithography must be developed.

In recent years, simple and low-cost methods for microlens array fabrication without photolithography have been reported. An ink-jet process using a drop-on-demand printer has been applied for the direct formation of microlens arrays on substrates [12, 13]. Microlens arrays can also be fabricated directly by pressing organic compounds onto a negative mold with micro-dimple structures [14, 15]. However, the microlens arrays fabricated by these processes are generally made of polymer materials including polydimethylsiloxane (PDMS) and polymethylmethacrylate (PMMA), and it is difficult to use polymer lens arrays in high-temperature environments such as those created by heat dissipation in electronic devices due to the deformation and decomposition of polymers under these conditions. Hence, transparent oxides, including silicon dioxide (SiO_2) and aluminum oxide (Al_2O_3), with heat-resistant properties may be suitable microlens materials.

The authors have recently demonstrated a novel method for fabricating micro- and nano-structures by laser irradiation and electrochemical techniques [16]. In this technique, an aluminum specimen covered with anodic oxide film is irradiated with a pulsed neodymium-doped yttrium aluminum garnet (Nd-YAG) laser to remove the oxide film locally, and then metals and organic compounds are deposited by electroplating, electroless plating, or electrophoretic deposition in areas where the oxide film has been removed by laser irradiation. Printed circuit boards [17, 18], plastic injection molds [19], 3D polypyrrole micro-manipulators [20-22], and other complicated 3D microstructures [23, 24] have been successfully fabricated by the technique. It has also been found that localized electrochemical etching and anodizing after laser irradiation allows for the formation of micropores [25], microgrooves [25], and semi-cylindrical oxides on metal substrates [26, 27]. It is important in both bottom-up and bottom-down fabrication processes to be able to form anodic oxide micro-patterns on the aluminum surface by laser irradiation and electrochemical techniques without photolithography. This technique may allow for the fabrication of anodic alumina microlens arrays with well-defined curvature under optimal fabrication conditions.

The aim of this study was to establish a technique for the fabrication of microlens arrays composed of anodic alumina by anodizing, laser irradiation, electropolishing, and re-anodizing. The effects of the conditions of laser irradiation, electropolishing, and anodizing on the shape and size of the resulting microstructures were investigated. In addition, a well-defined and high-density anodic alumina microlens array was fabricated to demonstrate the capabilities of the technique.

2. Experimental

The fabrication process of an alumina microlens array by laser irradiation and electrochemical techniques is shown in Fig. 1. Highly pure aluminum plates (99.99 wt%, 400 μm thick, Nippon Light Metal Co., Japan) were cut into 30 mm x 20 mm pieces with a handle and then ultrasonically degreased in an ethanol solution for 10 min. After degreasing, the specimens were electropolished in a 13.6 M

CH_3COOH / 2.56 M $HClO_4$ solution (T = 280 K) at a constant voltage of 28 V for 150 s. During the electropolishing, an aluminum plate was used as the counter electrode, and the solution was stirred slowly with a magnetic stirrer. The electropolished specimens were immersed in a 0.22 M $(COOH)_2$ solution (T = 293 K) and then anodized for 3 - 30 min at a constant current density of 100 A m^{-2} to form a porous anodic oxide film measuring 1 - 10 μm in thickness on the aluminum substrate (Fig. 1a). After anodizing, some specimens were boiled in doubly distilled water (T = 373 K) for 5 - 60 min to seal the nanopores in the porous oxide film.

The anodized specimens were immersed in doubly distilled water (T = 295 K) and then irradiated with a pulsed Nd-YAG laser to remove the anodic oxide film locally (Fig. 1b). Fig. 2 shows a schematic model of the laser irradiation setup used in this study. The laser beam (GCR-130-10, Spectra Physics) had a wavelength of 532 nm (second harmonic generation), pulse width of 8 ns, frequency of 10 Hz, and beam divergence of <0.5 mrad (full angle), and the laser power was adjusted to 0.5 - 1.0 mW during laser irradiation. The specimens were set in the focal position of the laser beam that passed through an iris diaphragm (Sigma-64, Sigma Koki Co., Japan), a convex lens with a 60 mm focal length (SLQ-15-60P, Sigma Koki Co.), and a quartz window. The specimens were irradiated with the laser for 0.5 - 2.0 s to form a micropore in the anodic oxide film. To control the position of the specimens during laser irradiation, the specimens were moved with a PC-controlled XY-stage (CPC-2DN, Chuo Precision Industrial Co., Japan). Laser irradiation in distilled water results in micromachining without debris around laser-irradiated areas [25].

After laser irradiation, the specimens were immersed in a 13.6 M CH_3COOH / 2.56 M $HClO_4$ solution (T = 280 K) and then electropolished at a constant voltage of 30 V to form a micropore with a flat surface (Fig. 1c). The aluminum exposed to the solution is preferentially dissolved by electropolishing, and the anodic oxide film remaining in areas not subjected to laser irradiation, which acts as an insulating mask during electropolishing in the $CH_3COOH/HClO_4$ solution, is attacked by the solution. To determine the optimal dissolution conditions for the electropolishing, the specimens completely covered with a porous oxide film with/without pore-sealing were also anodically polarized, and the time variations in the anodic current density were measured. In addition, the rest potentials of the anodized and pore-sealed specimens with different sealing times were measured by a potentiostat (PS-14, Toho Technical Research Co., Japan) during the immersion. A saturated KCl-Ag/AgCl electrode was used as a reference electrode in the rest potential measurements.

After electropolishing, the specimens were immersed in a 0.20 M CrO_3 / 0.54 M H_3PO_4 solution (T = 353 K) for 5 min to completely dissolve the anodic oxide film (Fig. 1d). The specimens were again immersed in a 0.22 M $(COOH)_2$ solution (T = 293 K) and then re-anodized for 60 min at a constant voltage of 50 V to form a porous oxide film with concave curvature (Fig. 1e). During constant voltage re-anodizing, the voltage was increased at 0.2 V s^{-1} during the initial period until 50 V was reached; the specimens were then maintained at this voltage. Finally, the anodized specimens were immersed in a 0.32 M $SnCl_4$ solution at room temperature to completely dissolve the aluminum substrate (Fig. 1f), and an anodic alumina thin film with a microlens array was obtained.

The structural changes induced in the specimens by laser irradiation and each electrochemical process were examined by scanning electron microscopy (SEM, Miniscope TM-1000, Hitachi), electron probe microanalysis (EPMA, JXA-8900M ED/WD, JEOL), and confocal scanning laser microscopy (CSLM, 1SA21, Lasertec). To observe their vertical cross-section, the specimens were embedded in an epoxy resin, polished mechanically, and then immersed in a 0.25 M $K_3[Fe(CN)_6]$ / 4.17 M NaOH solution at room temperature for 20 s to clearly observe the nanoporous layer in the anodic oxide. The polished specimens were sputter-coated with platinum using a sputter coater (JFC-1600, JEOL) for SEM observations.

3. Results

3.1 Effect of pore-sealing on electrochemical resistance in $CH_3COOH/HClO_4$ solution

The immersion of a porous anodic oxide film formed on an aluminum specimen in distilled boiling water results in the hydration of the oxide via the following chemical reaction [28-30]:

$$Al_2O_3 + nH_2O = Al_2O_3\,nH_2O \quad (1)$$

During immersion, most of the hydration occurs in the outermost part of the porous layer, where highly crystalline hydroxide layers are formed. Accordingly, the nanopores in the anodic oxide film are sealed with the hydroxide. In general, it is a well-known experimental fact that the pore-sealing process improves the electrochemical resistance of the anodic oxide film in acid and alkaline solutions. As mentioned previously, in the microlens array fabrication method used in this work, the non-irradiated areas of the anodic oxide films act as insulating masks during electropolishing (Fig. 1c). Therefore, the electrochemical resistance of the anodic oxide film was examined to determine the optimal conditions for anodizing, pore-sealing, and electropolishing.

Fig. 3 shows the changes in the current density, i, with time, t_p, during anodic polarization with the anodized aluminum specimen in a 13.6 M CH_3COOH / 2.56 M $HClO_4$ solution. Before polarization, the aluminum specimen was covered with a porous anodic oxide film (1μm thickness) and then pore-sealed in distilled water at 373 K for periods of a) 0, b) 5, c) 15, and d) 60 min. The specimen was immersed in a $CH_3COOH/HClO_4$ solution and then anodically polarized for 30 min at a constant voltage of 30 V during polarization. The current density increased with polarization time during each pore-sealing period after the initial transients, and this tendency was more marked at longer pore-sealing times. The current density corresponds to dissolved aluminum ions carried through imperfections in the oxide layer:

$$Al = Al^{3+} + 3e^- \quad (2)$$

It is clear from Fig. 3 that the anodic oxide film without pore-sealing shows relatively high electrochemical resistance in $CH_3COOH/HClO_4$, although a slight current density of approximately 1.0 – 1.5 mA m^{-2} was measured during polarization. This incomplete insulation of the anodic oxide film in the solution will be permitted for nanolens array fabrication because the value of the current density is very low. In addition, because the aluminum substrate without the oxide mask is exposed to the solution by laser irradiation (Fig. 1c), the dissolution of the aluminum substrate will occur preferentially in the laser-irradiated area during electropolishing. The reason why the electrochemical resistance of the anodic oxide film decreased with the pore-sealing time will be addressed in the discussion section.

3.2 Laser irradiation and subsequent electropolishing of the aluminum covered with anodic oxide film

An aluminum specimen covered with a porous anodic oxide film (1 μm thickness) without pore-sealing was irradiated with a pulsed YAG laser to remove the oxide film in distilled water. Fig. 4a shows an SEM image of the surface of the specimen irradiated at a laser power P = 1 mW for an irradiation time t_i = 2 s. The circular micropore shown in Fig. 4a corresponds to the laser-irradiated area and the gray part around the pore to the anodic oxide film that was not irradiated. It can be seen from Fig. 4a that the anodic oxide film was removed from the specimen by laser irradiation, and many cracks were formed around the laser-irradiated area. A three-dimensional CSLM height image showed that the thin anodic oxide film was completely removed by laser irradiation, and the aluminum substrate, with a depth of approximately 20 μm at the center of the laser-irradiated area, was exposed. Fig. 4b shows an SEM image of a specimen irradiated at P = 0.5 mW for t_i = 0.5 s. The oxide film was also removed locally, and the exposed aluminum substrate shows an uneven surface, like that of a milk crown, due to the rapid melting and solidification of the aluminum by laser irradiation. However, no crack was observed around the removed area of the anodic oxide. Fig. 4 clearly shows that long-term laser irradiation with high laser power resulted in the formation of cracks around the laser-irradiated area.

The mechanism of anodic oxide removal is based on that of laser ablation [16, 25]. A laser beam passed through the transparent anodic oxide film and reaches the interface between the oxide and aluminum substrate. The laser beam heats the aluminum to form a plasma, which removes the oxide film due to the high pressure between the oxide and aluminum. The melted aluminum substrate is rapidly quenched in water after the oxide removal, and micropores, shown in Fig. 4, are formed.

Fig. 5 shows SEM images of the surface of electropolished specimens in a $CH_3COOH/HClO_4$ solution for 5 min after laser irradiation. Laser irradiation was carried out a) at P = 1 mW for t_i = 2.0 s and b) at 0.5 mW for 0.5 s (see Fig. 4). Comparing Fig. 5a with 4a shows that irregularly shaped micropore with different diameters (vertical and horizontal directions) is fabricated by electropolishing, although the exposed aluminum substrate shows a smooth surface. In addition, a light-gray oxide film with a width of approximately 10 μm can be observed around the pore. This is a free-standing oxide film, whose formation can be explained as the result of undercutting, which occurs under the oxide film by isotropic electrochemical dissolution [31, 32]. In fact, CSLM revealed a space under the light-gray oxide. In contrast, electropolishing of the specimen shown in Fig. 4b led to the formation of a circular pore with a free-standing oxide film around the pore (Fig. 5b). No electrochemical dissolution of aluminum was observed at the non-irradiated area by SEM or optical microscopy: this suggests that the anodic oxide film without pore-sealing exhibits good insulating properties during electropolishing in the $CH_3COOH/HClO_4$ solution, as shown in Fig. 3.

The anodic polarization of aluminum in a $CH_3COOH/HClO_4$ solution, which is normally used as an electropolishing solution for aluminum and iron, results in the microsmoothing of the surface [33, 34]. The aluminum dissolves rapidly to the solution during the initial stage of electropolishing, and a highly concentrated electrolyte layer is formed on the surface during electropolishing. Under these mass-transport limitations, micrometer-scale convex regions on the aluminum surface preferentially dissolve to the solution. Therefore, the aluminum surface is smoothed by electropolishing on a microscopic level, as shown in Fig. 5.

As shown in Figs. 4 and 5, circular micropores with smooth surfaces can be fabricated on aluminum substrate by laser irradiation and electropolishing under optimal conditions, although in this study, a free-standing oxide film was also formed around the pores. The diameter and depth of the pores formed by electropolishing increased with the etching time, thus allowing for size control.

3.3 Re-anodizing of the electropolished specimens

After being electrochemically polished, the specimen was immersed in CrO_3/H_3PO_4 solution to completely dissolve the anodic oxide film, which formed a free-standing layer and still remained on the aluminum substrate (Fig. 1d). Fig. 6a shows an SEM image of the vertical cross-section of the specimen after the dissolution of the oxide film. Here, the gray region at the bottom corresponds to the aluminum substrate and the black region at the top to an epoxy resin. A semi-elliptical micropore measuring 60 μm in diameter and 25 μm in depth was observed, and it is clear that the free-standing oxide formed by electropolishing was dissolved by immersion in the CrO_3/H_3PO_4 solution.

Fig. 6b shows an SEM image of the vertical cross-section of a specimen that was re-anodized for 60 min in a $(COOH)_2$ solution at a constant voltage of 50 V. The gray layer between the epoxy resin and aluminum substrate is the porous oxide film formed by re-anodizing, and the anodic oxide grew on the semi-elliptical micropore as well as on the flat surface. It should be noted that the thickness of the oxide film on the semi-elliptical micropore is different at each position. Figs. 6c and 6d show high-magnification SEM images of the boxed regions indicated in Fig. 6b. Striped patterns are observed in Figs. 6c and 6d due to the formation of many nanopores in the anodic oxide film. It is clear that the thickness of the oxide film at the pore bottom (12.2 μm, Fig. 6c) is thicker than that at the periphery (6.7

μm, Fig. 6d), and the anodic oxide becomes thinner in the direction of the periphery from the pore bottom (Fig. 6b). This strongly suggests that the growth rate of the oxide film depends on the position of semi-elliptical pores in the aluminum substrate. The characteristic oxide film formed on the semi-elliptical micropore is shaped like a positive meniscus lens, which consists of a steep convex surface. Fig. 7 shows the a) aluminum and b) oxygen element distributions obtained by EPMA analysis of the area shown in Fig. 6b, and the scales to the right of the images indicate the relative intensities of aluminum and oxygen. By comparing the aluminum and oxygen distributions, EPMA studies show that the elements are distributed evenly in the anodic oxide film. The distinctive shape of the oxide film on the semi-elliptical pore will be addressed in the discussion section.

3.4 Fabrication of alumina microlens array

After re-anodizing, as shown in Fig. 6, the anodic oxide film formed on the backside of the specimen was removed from the aluminum substrate by chemical dissolution or mechanical polishing. Therefore, the aluminum substrate on the backside was exposed by film removal. The specimen was then immersed in a 0.32 M $SnCl_4$ solution to completely dissolve the aluminum substrate (Fig. 1f). Hydrogen gas evolved during the immersion, and the aluminum substrate, measuring 400 μm in thickness, was completely dissolved within 2 min. A transparent thin anodic oxide film was obtained in the solution after hydrogen gas evolution.

Fig. 8a shows an SEM image of the anodic alumina microlens array obtained by the dissolution of the aluminum substrate. It is clear that many microlenses were successfully fabricated on the anodic oxide film. The microlenses measure approximately 40 μm in diameter and are spaced at 60 μm intervals. No crack or imperfections were observed on the anodic oxide film after it was lifted off from the aluminum substrate. Figs. 8b and 8c reveal the convex shape of the microlenses, although the anodic oxide substrate around the lenses is slightly hollow (Fig. 8c); these hollow regions were observed at the edge of the oxide formed on the semi-elliptical micropores (Figs. 6b, 6d, and 7). The anodic oxide thin film was flexible, and no thermal deformation was observed following heat treatment at 773 K for 2 h without an amorphous-to-crystalline transition. These advantages suggest that the anodic oxide film is a suitable material for microlens arrays. Such microlenses fabricated on anodic alumina can be used as positive meniscus lens arrays.

A high-density anodic alumina microlens array was successfully fabricated by laser irradiation and electrochemical techniques. The diameter of the anodic alumina microlenses was determined to be 37.6 to 42.3 μm by precise shape measurement at different microlenses. A diameter difference may be caused by slight difference in the shapes of the film-removed area fabricated by laser irradiation. The difference, however, will be improved by choosing the optimal conditions for laser irradiation. The authors have already succeeded in fabricating oxide-removed patterns with features measuring approximately 5 μm in diameter [17]; thus, the fabrication of smaller alumina microlens arrays should be possible. However, the fabrication process proposed in this investigation requires several electrochemical steps such as anodizing, electropolishing, re-anodizing, and dissolution of oxide/aluminum. Therefore, a simpler technique for creating alumina microlens arrays should be developed. Recently, the authors developed a new method for fabricating well-defined alumina microlens arrays using an imprint technique with a mold. This method will be reported in the near future. Nanopores formed in a porous anodic oxide film may have no effect on the focus profile of meniscus microlenses because the diameter of each nanopore formed in an oxalic acid solution (approximately 60 nm) is sufficiently smaller than the wavelength of visible light [35]. However, the optical characteristics of these alumina microlens arrays should be further investigated for micro-optical device applications.

4. Discussion

4.1 Decrease in the electrochemical resistance of the anodic oxide film after pore-sealing

As described in Section 3.1, pore-sealing of the porous anodic oxide film reduces the film's electrochemical resistance in a $CH_3COOH/HClO_4$ solution, though the authors strongly expected the oxide film to exhibit good resistance after pore-sealing. To further study the electrochemical resistance of the anodic oxide, the rest potentials of the specimen covered with the oxide film were measured in a $CH_3COOH/HClO_4$ solution.

Fig. 9 shows the changes in the rest potential of the anodized and pore-sealed specimens, E, with immersion time, t_i, in a $CH_3COOH/HClO_4$ solution at 280 K. The aluminum specimen was anodized in a $(COOH)_2$ solution for 10 min, and the pore-sealing conditions of all specimens were the same as those described in Section 3.1. In Fig. 9, the rest potential is described as a mixed potential of the following anodic and cathodic reactions:

$$Al = Al^{3+} + 3e^- \quad \text{(Anodic reaction)} \quad (3)$$

$$2H^+ + 2e^- = H_2 \quad \text{(Cathodic reaction)} \quad (4)$$

The anodic reaction occurs on the substrate at defects in the anodic oxide film, while the cathodic reaction is believed to occur over nearly the entire surface of the substrate because protons easily migrate through the oxide film [26]. Hence, the open-circuit rest potential strongly depends on the number of defects in the oxide film, and the rest potential increases with increasing chemical resistance due to the decrease in the number of defects [26]. It is clear from Fig. 9 that each rest potential drops with immersion time during the initial stage to reach steady values, and the rest potential gradually shifts to more negative potentials with pore-sealing time. Rest potential measurements were also performed using aluminum specimens with different oxide thicknesses. The measured rest potentials showed a tendency to shift to more negative values with pore-sealing time. The rest potential measurements strongly suggest that the resistance of the anodic oxide film becomes lower with increasing pore-sealing time, in agreement with the results shown in Fig. 3.

A porous anodic oxide film with nanopores can be formed on aluminum by anodizing in acid solutions [36-43]. The oxide film consists of numerous fine hexagonal cells perpendicular to the substrate and each cell has a nanopore at its center. The pores are separated from the aluminum substrate by a thin barrier layer. Pore-sealing results in the sealing of the nanopores with hydroxides (see eq. 1): accordingly, the barrier layer at the pore bottom becomes thinner with increasing pore-sealing time [44]. This thinning phenomenon of the barrier layer may be due to a decrease in electrochemical dissolution resistance, if the hydroxides have a pathway to penetrate the barrier layer from the concentrated $CH_3COOH/HClO_4$ solution. However, further studies by transmission electron microscopy (TEM) and electrochemical impedance spectroscopy (EIS) are required to understand the electrochemical resistance of the anodic oxide film in a $CH_3COOH/HClO_4$ solution.

4.2 Growth behavior of the anodic oxide film on semi-elliptical pore

The growth behavior of the anodic oxide film on a semi-elliptical pore formed by laser irradiation and electropolishing was described in Section 3.3, and the results show that a meniscus-shaped oxide film grew on the semi-elliptical pore. The mechanism of formation will now be discussed. Fig. 10 shows a schematic model of the growth of the oxide film on the semi-elliptical pore by re-anodizing. At the semi-elliptical pore bottom, the nanopores in the porous oxide grows perpendicularly to the substrate because the aluminum substrate has a nearly flat surface. In contrast, at the periphery of the semi-elliptical pore, the porous oxide may have a microscopic pore-branching structure that is similar to that obtained by previous studies [45-47] the aluminum substrate has a large curvature, as shown in Fig. 6b. The branching of the nanopores reduces the oxide growth rate at the barrier layer because the

diffusion of chemical species such as hydrogen, oxalate, and aluminum ions in the nanopores gradually becomes more difficult. Therefore, the curvatures at the top and bottom of the meniscus-shaped oxide formed on the semi-elliptical pore may be different, as shown in Fig. 6.

5. Conclusions

An anodic alumina microlens array was fabricated by aluminum anodizing, laser irradiation, electropolishing, re-anodizing, and lift-off of the thin oxide film. The following conclusions may be drawn from results of the electrochemical measurements and microfabrication performed in this study.

(1) A porous anodic oxide film without pore-sealing has good insulating properties during electropolishing in a $CH_3COOH/HClO_4$ solution; the pore-sealing treatment of the oxide film, however, increases the anodic current density through the oxide film.

(2) A micropore can be fabricated on an aluminum substrate by anodizing, laser irradiation, and electropolishing. Subsequent re-anodizing results in the formation of meniscus-shaped anodic oxide on the micropore due to the difference in the oxide growth rate between the periphery and bottom of the pore.

(3) A flexible microlens array composed of an anodic alumina film can be lifted off from the aluminum substrate by the chemical dissolution of aluminum in a $SnCl_4$ solution. The microlenses have a cross-sectional profile that is semi-elliptical in shape.

Acknowledgements

The authors would like to thank Mr. Nobuyuki Miyazaki (Hokkaido University) for his assistance in the EPMA analysis. This work was financially supported by the Japan Society for the Promotion of Science (JSPS) “KAKENHI”.

References

1) T. K. Shih, C. F. Chen, J. R. Ho, F. T. Chuang, Microelectron. Eng. 83 (2006) 2499.
2) M. Ashraf, C. Gupta, F. Chollet, S. V. Springham, R. S. Rawat, Opt. Lasers Eng. 46 (2008) 711.
3) C. T. Pan, M. F. Chen, P. J. Cheng, Y. M. Hwang, S. D. Tseng, J. C. Huang, Sens. Actuat. A 150 (2009) 156.
4) J. Xia, D. Qu, H. Yang, J. Chen, W. Zhu, Displays 31 (2010) 186.
5) C. T. Pan, Y. C. Chen, M. F. Chen, Y. C. Hsu, Opt. Commun. 284 (2011) 3323.
6) C. H. Chien, C. T. Pan, C. C. Hsieh, C. M. Yang, K. L. Sher, Sens. Actuat. A 122 (2005) 55.
7) C. K. Chung, Y. Z. Hong, Microsyst. Technol. 13 (2007) 523.
8) W. Daschner, P. Long, R. Stein, C. Wu, S. H. Lee, J. Vac. Sci. Technol. B 14 (1996) 3730.
9) H. Jiang, X. Yuan, Z. Yun, Y. C. Chan, Y. L. Lam, Mater. Sci. Eng. C 16 (2001) 99.
10) J. J. Yang, Y. S. Liao, C. F. Chen, Opt. Commun. 270 (2007) 433.
11) H. Yoshida, T. Kataoka, M. Tanaka, J. Non-Cryst. Solids 112 (1989) 352.
12) R. Danzebrink, M. A. Aegerter, Thin Solid Films 392 (2001) 223.
13) F. T. O’Neill, G. Owen, J. T. Sheridan, Optik 116 (2005) 158.
14) C. Y. Chang, S. Y. Yang, L. S. Huang, J. H. Chang, Inf. Phys. Technol. 48 (2006) 163.
15) T. Yanagishita, K. Nishio, H. Masuda, Appl. Phys. Express 2 (2009) 022001.
16) T. Kikuchi, S. Z. Chu, S. Jonishi, M. Sakairi, H. Takahashi, Electrochim. Acta 47 (2001) 225.
17) T. Kikuchi, M. Sakairi, H. Takahashi, Y. Abe, N. Katayama, Surf. Coat. Technol. 169-170C (2003) 199.
18) H. Jha, T. Kikuchi, M. Sakairi, H. Takahashi, ACS Appl. Mater. Interfaces 2 (2010) 774.
19) S. M. Moon, M. Sakairi, H. Takahashi, K. SHimamura, Electrochemistry 71 (2003) 260.

20) Y. Akiyama, T. Kikuchi, M. Ueda, M. Iida, M. Sakairi, H. Takahashi, Electrochim. Acta 51 (2006) 4834.
21) T. Kikuchi, Y. Akiyama, M. Ueda, M. Sakairi, H. Takahashi, Electrochim. Acta 52 (2007) 4480.
22) T. Kikuchi, S. Ueda, M. Ueda, M. Sakairi, H. Takahashi, J. Surf. Fin. Soc. Jpn. 60 (2009) 335.
23) T. Kikuchi, M. Sakairi, H. Takahashi, J. Electrochem. Soc. 150 (2003) C567.
24) T. Kikuchi, H. Takahashi, T. Maruko, Electrochim. Acta 52 (2007) 2352.
25) T. Kikuchi, M. Sakairi, H. Takahashi, Y. Abe, N. Katayama, J. Electrochem. Soc. 148 (2001) C740.
26) T. Kikuchi, M. Sakairi, H. Takahashi, Electrochim. Acta 54 (2009) 7018.
27) H. Jha, T. Kikuchi, M. Sakairi, H. Takahashi, J. Micromech. Microeng. 17 (2007) 1949.
28) J. P. Hoar, G. C. Wood, Electrochim. Acta 7 (1962) 333.
29) J. P. O'Sullivan, G. C. Wood, J. Electrochem. Soc. 116 (1969) 1351.
30) M. Koda, H. Takahashi, S. Nagayama, J. Surf. Finish. Soc. Jpn. 33 (1982) 242.
31) C. Madore, O. Piotrowski, D. Landolt, J. Electrochem. Soc. 146 (1999) 2526.
32) P. F. Chauvy, C. Madore, D. Landolt, Electrochem. Solid-State Lett. 2 (1999) 123.
33) P. A. Jacquet, Nature 135 (1935) 1076.
34) D. Landolt, Electrochim. Acta 32 (1987) 1.
35) H. Jha, T. Kikuchi, M. Sakairi, H. Takahashi, Nanotechnology 19 (2008) 395603.
36) H. Masuda, K. Fukuda, Science 268 (1995) 1466.
37) F. Keller, M. S. Hunter, D. L. Robinson, J. Electrochem. Soc. 100 (1953) 411.
38) G. E. Thompson, R. C. Furneaux, G. C. Wood, J. A. Richardson, J. S. Gode, Nature 272 (1978) 433.
39) S. Ono, M. Saito, M. Ishiguro, H. Asoh, J. Electrochem. Soc. 151 (2004) B473.
40) W. Lee, R. Ji, U. Gosele, K. Nielsch, Nature Mater. 5 (2006) 741.
41) S. Z. Chu, K. Wada, S. Inoue, M. Isogai, Y. Katsuta, A. Yasumori, J. Electrochem. Soc. 153 (2006) B384.
42) J. E. Houser, K. R. Hebert, Nature Mater. 8 (2009) 415.
43) K. R. Hebert, S. P. Albu, I. Paramasivam, P. Schmuki, Nature Mater. 11 (2012) 162.
44) M. Koda, H. Takahashi, M. Nagayama, J. Surf. Fin. Soc. Jpn. 33 (1982) 242.
45) T. A. Renshaw, J. Electrochem. Soc. 108 (1961) 185.
46) H. Takahashi, M. Nagayama, H. Akahori, and A. Kitahara, J. Electron Microscopy 22 (1973) 149.
47) C. Chung, M. Liao, C. Lee, H. Chang, Nano. Res. Lett. 6 (2011) 569.

Captions

Fig. 1 Schematic models for alumina microlens array fabrication. a) Anodizing of aluminum to form an oxide film on the aluminum substrate. b) Laser irradiation to remove the oxide film. c) Electrochemical polishing of aluminum substrate. d) Dissolution of oxide film in chromic and phosphoric acid solution mixture. e) Anodizing again to form an oxide film with a lens configuration. f) Aluminum substrate dissolution in tin chloride solution.

Fig. 2 Schematic model of laser irradiation setup.

Fig. 3 Changes in anodic current density, i, with anodic polarization time, t_p, in 13.6 M CH_3COOH / 2.56 M $HClO_4$ solution (280 K) using an aluminum specimen covered with porous anodic oxide film measuring 1 μm in thickness. Before polarization, the specimens were immersed in distilled water for t_s = a) 0, b) 5, c) 15, and d) 60 min for pore-sealing.

Fig. 4 SEM images of the surface of anodized specimen after laser irradiation a) at P = 0.5 mW for t_i = 0.5 s and b) at P = 1 mW for t_i = 2.0 s. A porous anodic oxide film without pore-sealing was formed on the aluminum substrate.

Fig. 5 SEM images of the micropore fabricated by electropolishing for 5 min in $CH_3COOH/HClO_4$ solution after laser irradiation. Laser irradiation was carried out a) at 1 mW for t_i = 2.0 s and b) at 0.5 mW for t_i = 0.5 s.

Fig. 6 SEM images of the cross-section of specimens a) before and b) after re-anodizing for 60 min in $(COOH)_2$ solution. c), d) High-magnification SEM images of the specimen in the areas indicated by squares in Fig. 6b.

Fig. 7 EPMA-determined distributions of a) aluminum and b) oxygen in a cross-section of the re-anodized specimen. The scales to the right indicate the relative intensities of aluminum and oxygen.

Fig. 8 SEM images of the anodic alumina microlens array fabricated via anodizing, laser irradiation, electropolishing, re-anodizing, and substrate dissolution shown schematically in Fig. 1.

Fig. 9 Changes in the rest potential of anodized specimens, E, with immersion time, t_i, in 13.6 M CH_3COOH / 2.56 M $HClO_4$ solution (280 K). Anodizing was carried out for 10 min in 0.22 M $(COOH)_2$ solution at 293 K, and pore-sealing was performed by immersing in distilled boiling water for different pore-sealing times, t_ss.

Fig. 10 Schematic model illustrating the formation of the porous anodic oxide film with nanopores on semi-elliptical micropore by re-anodizing.

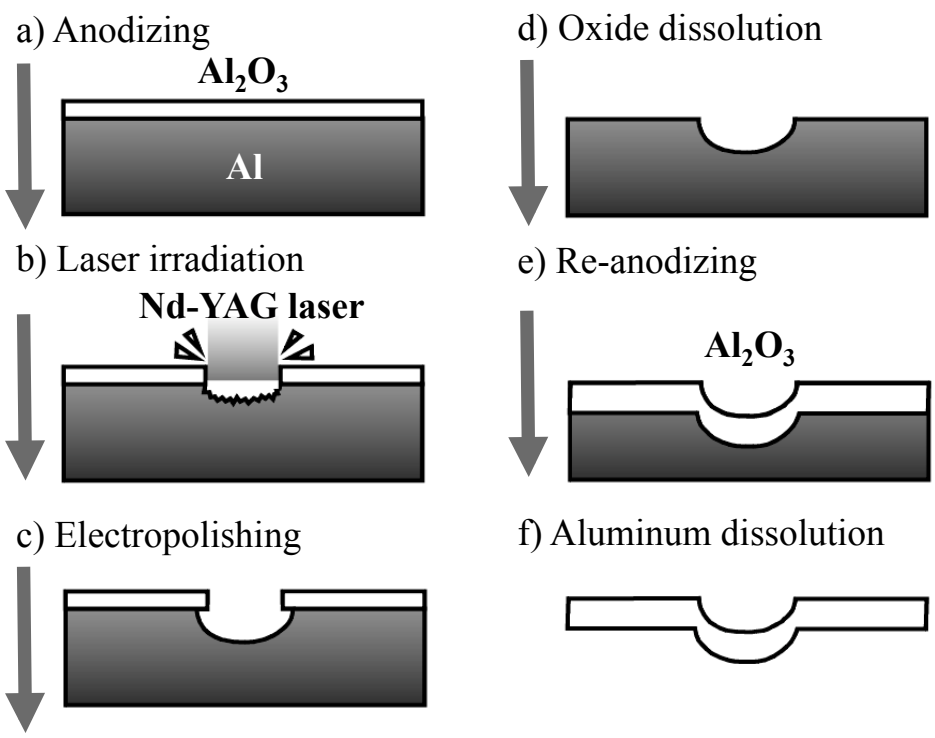
a) Anodizing
Al_2O_3
Al
b) Laser irradiation
Nd-YAG laser
c) Electropolishing
d) Oxide dissolution
e) Re-anodizing
Al_2O_3
f) Aluminum dissolution

Fig. 1

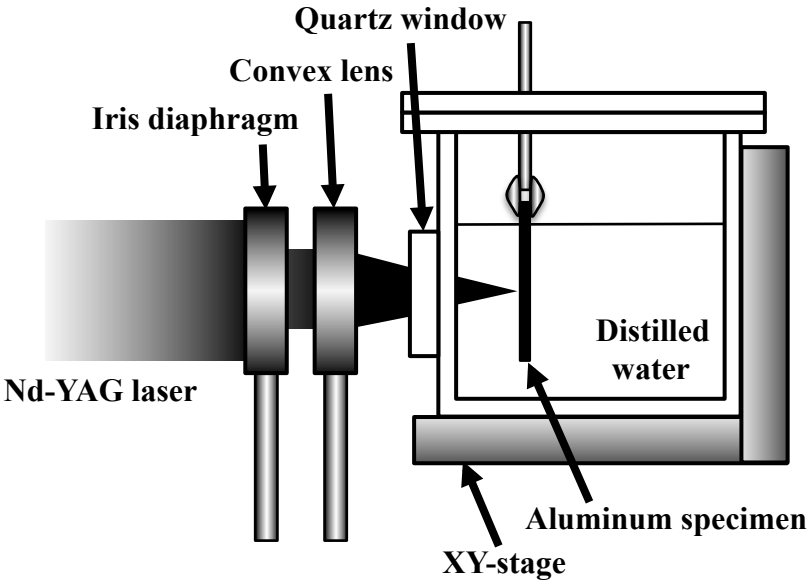
Quartz window
Convex lens
Iris diaphragm
Distilled
water
Nd-YAG laser
Aluminum specimen
XY-stage

Fig. 2

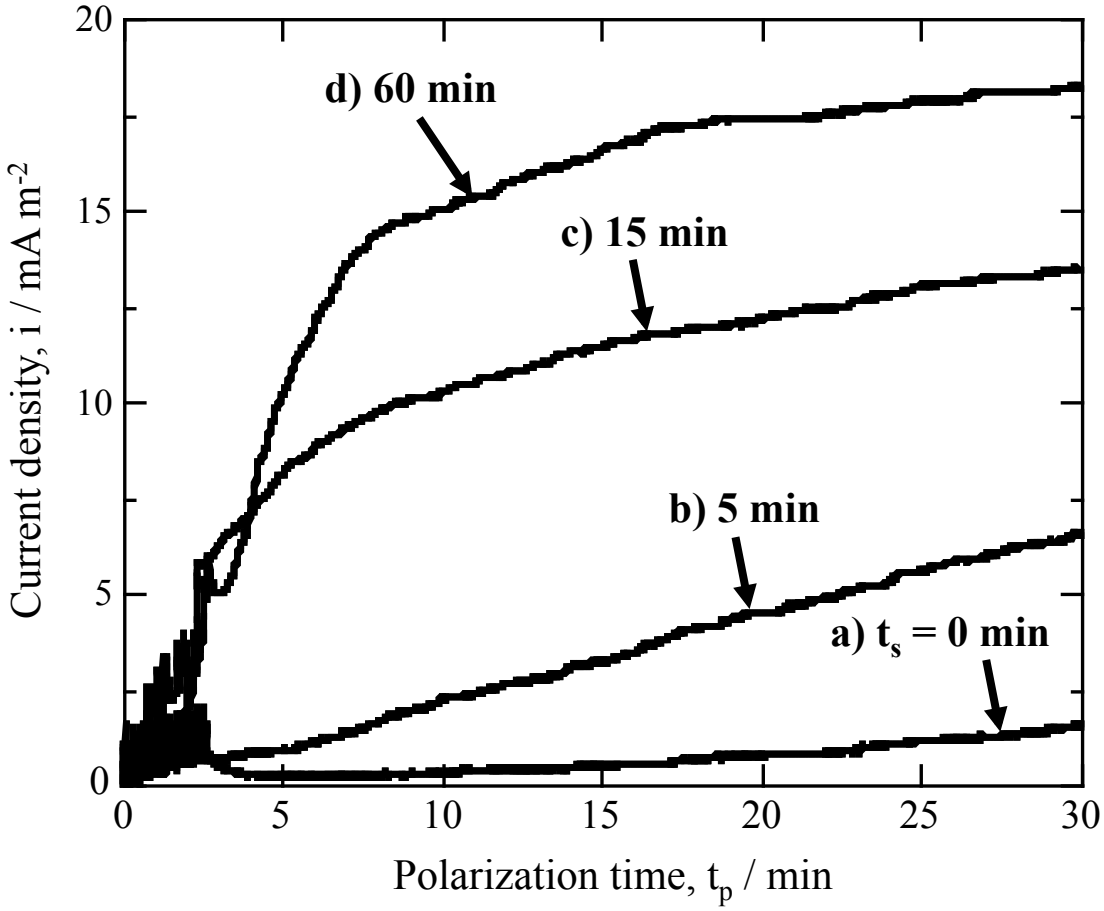
20
15
10
5
0
0
5
10
15
20
25
30
Current density, i / mA m-2
Polarization time, tp / min
d) 60 min
c) 15 min
b) 5 min
a) ts = 0 min

Fig. 3

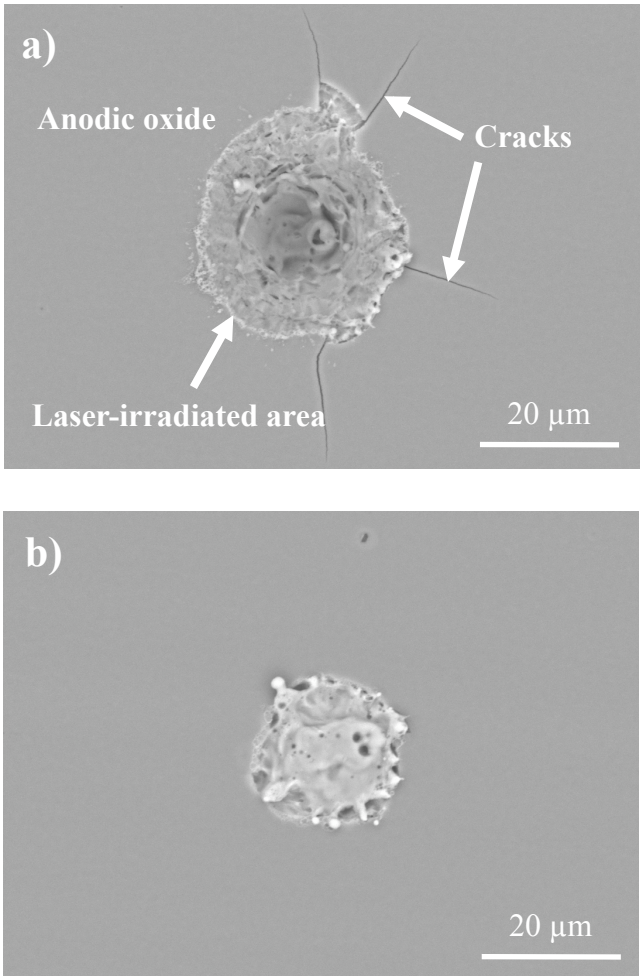

Fig. 4

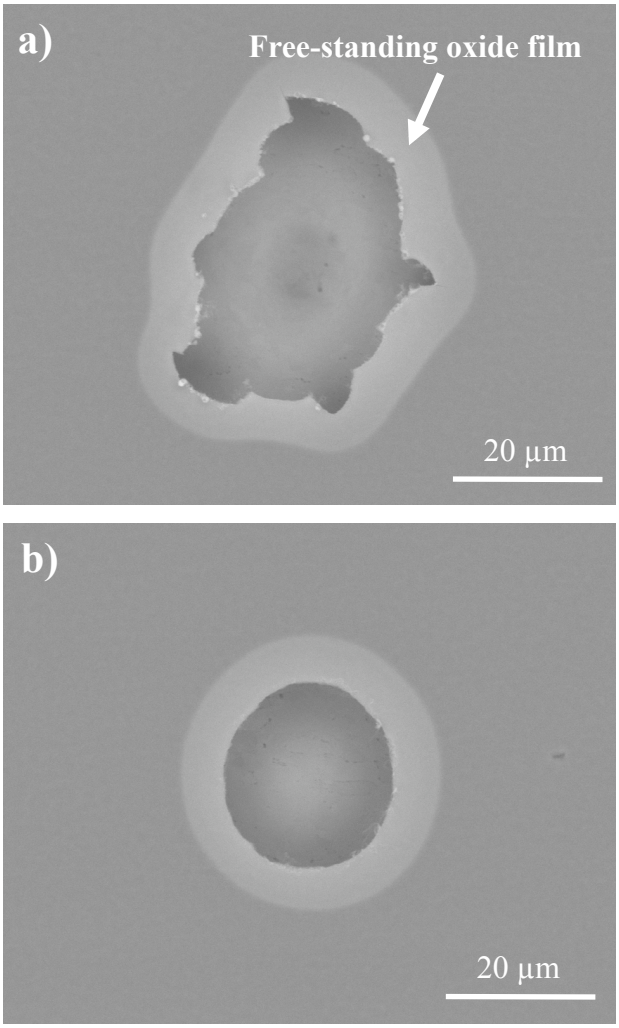

Fig. 5

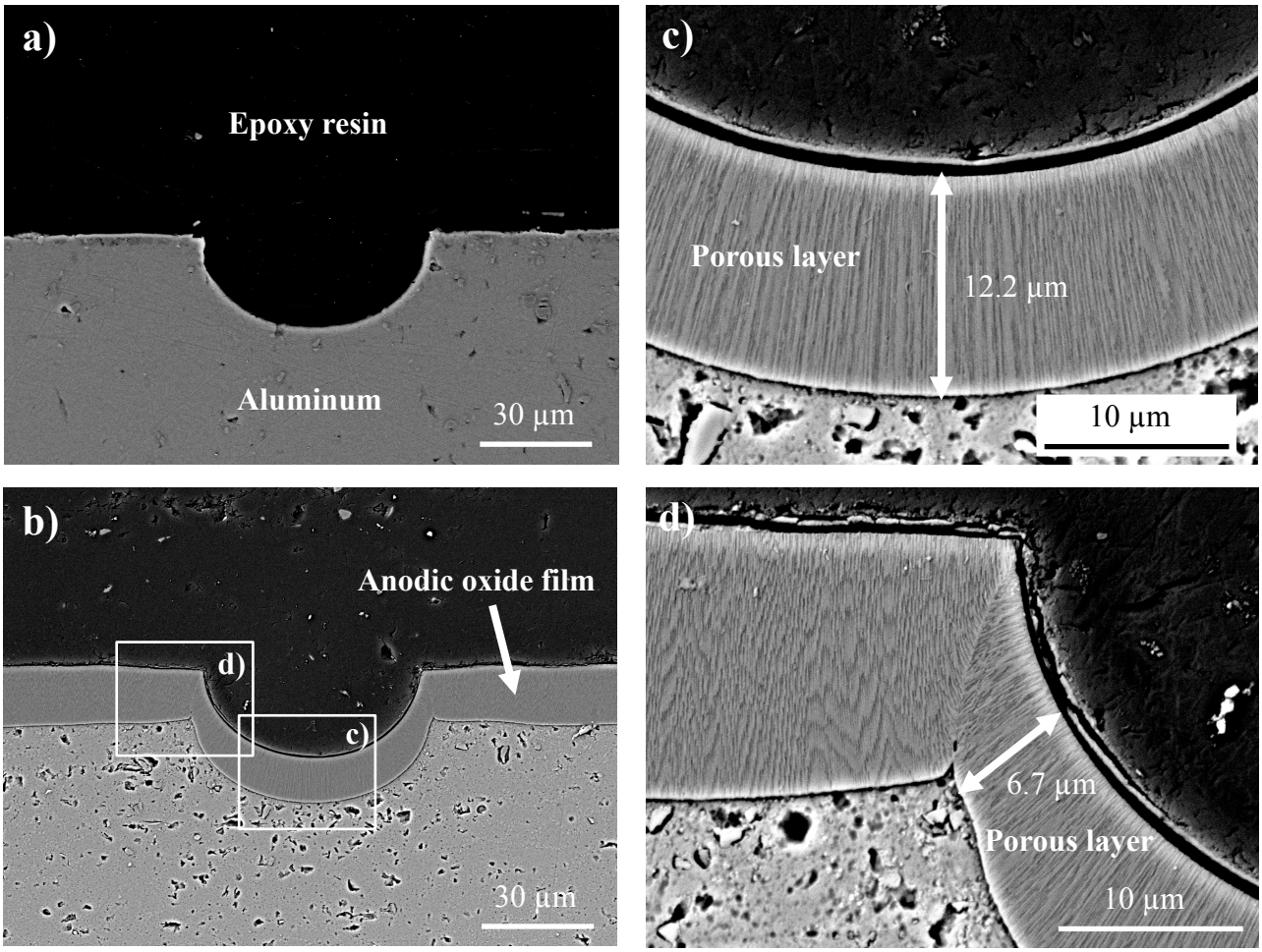
a)
Epoxy resin
Aluminum
30 μm
c)
Porous layer
12.2 μm
10 μm
b)
Anodic oxide film
d)
c)
30 μm
d)
6.7 μm
Porous layer
10 μm

Fig. 6

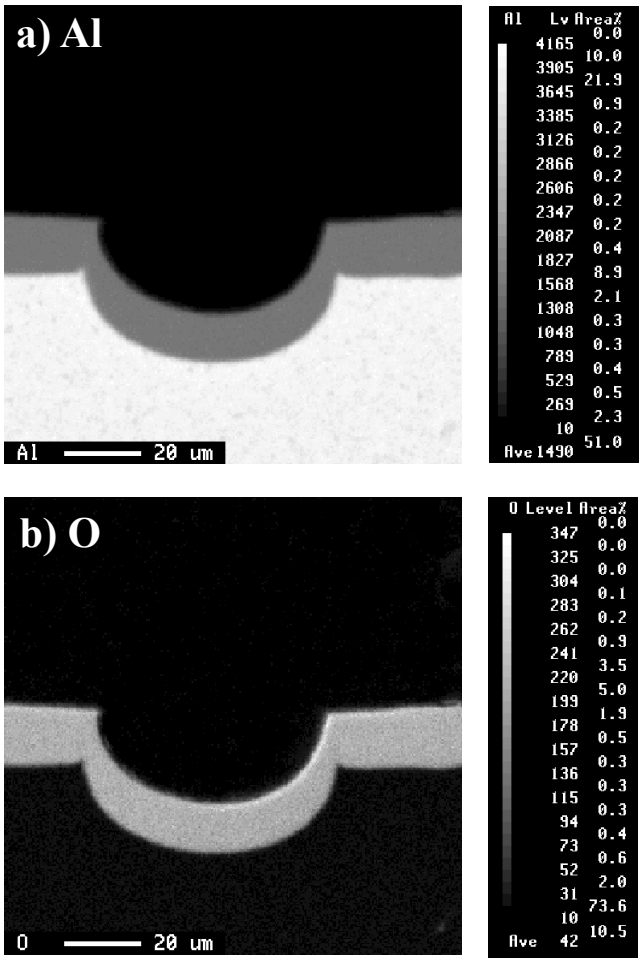
a) Al
Al 20 um
Al Lv AreaZ
4165 0.0
3905 10.0
3645 21.9
3385 0.9
3126 0.2
2866 0.2
2606 0.2
2347 0.2
2087 0.4
1827 8.9
1568 2.1
1308 0.3
1048 0.3
789 0.4
529 0.5
269 2.3
10 51.0
Ave 1490
b) O
O 20 um
O Level AreaZ
347 0.0
325 0.0
304 0.0
283 0.1
262 0.2
241 0.9
220 3.5
199 5.0
178 1.9
157 0.5
136 0.3
115 0.3
94 0.3
73 0.4
52 0.6
31 2.0
10 73.6
Ave 42 10.5

Fig. 7

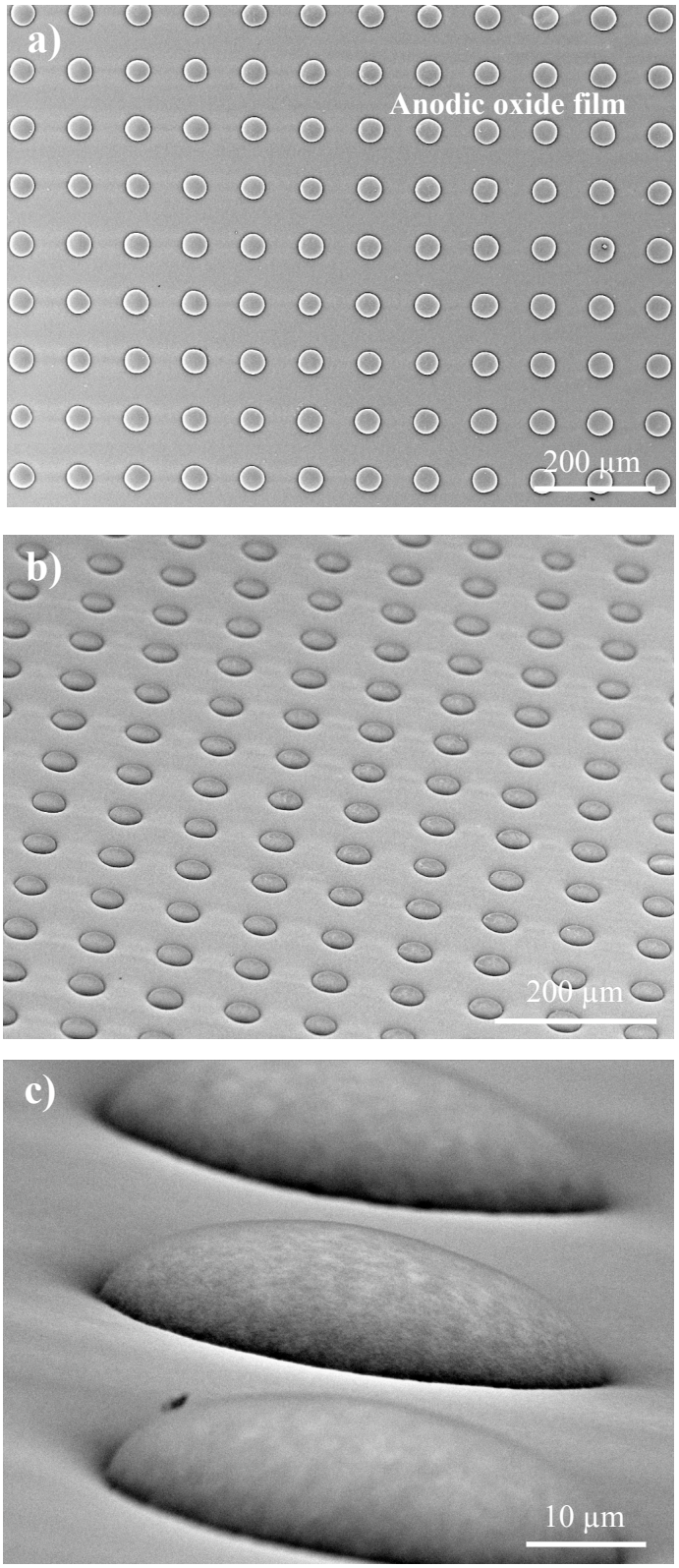

Fig. 8

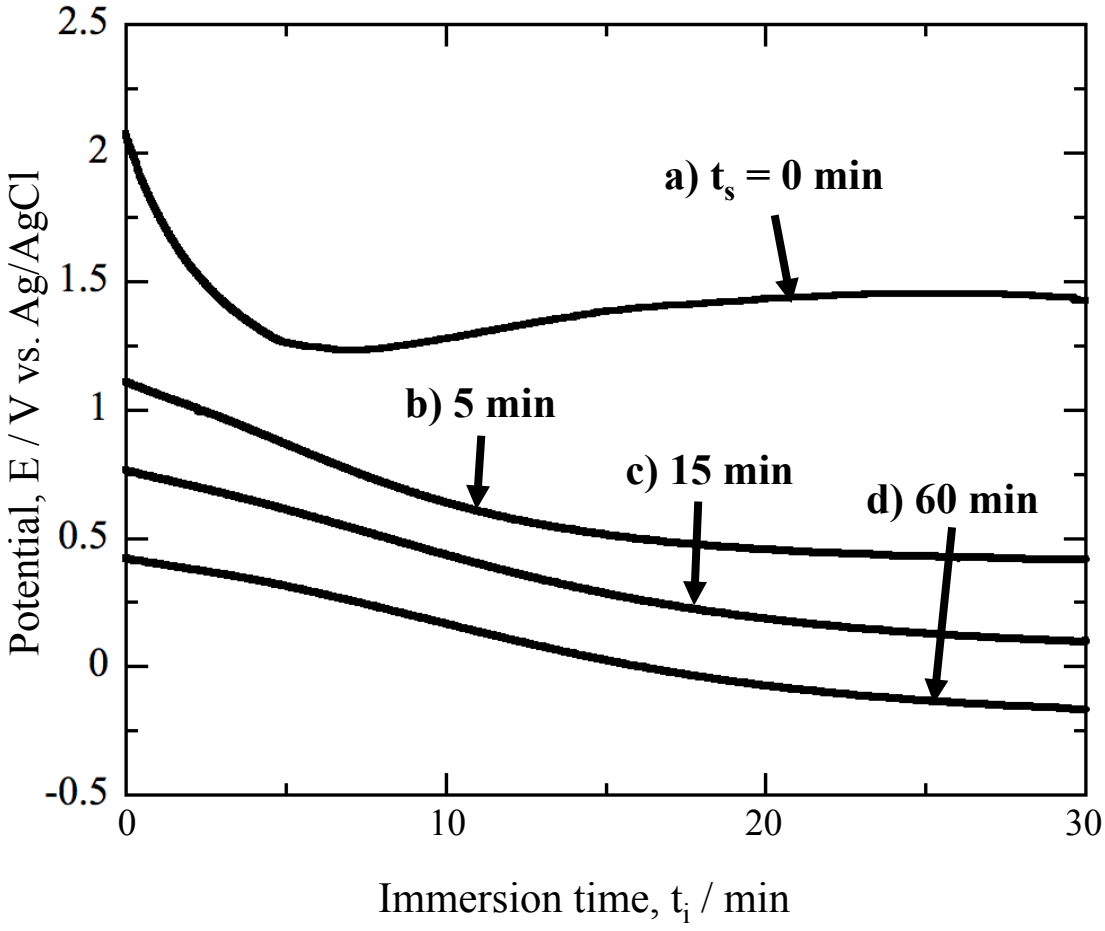
2.5
2
1.5
1
0.5
0
-0.5
0
10
20
30
Potential, E / V vs. Ag/AgCl
Immersion time, t_i / min
a) t_s = 0 min
b) 5 min
c) 15 min
d) 60 min

Fig. 9

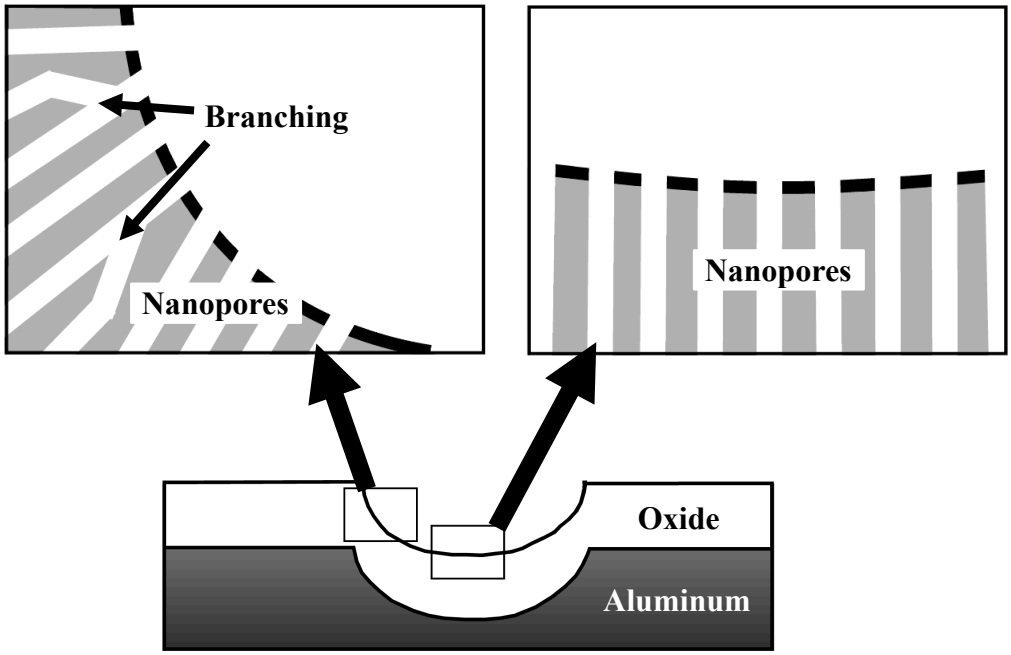

Fig. 10